

Attention-aware Generalized Mean Pooling for Image Retrieval

Yinzheng Gu

Chuanpeng Li

Jinbin Xie

Venvy Inc. (Video++)

{guyinzheng, lichuanpeng, xie}@videopls.com

Abstract

It has been shown that image descriptors extracted by convolutional neural networks (CNNs) achieve remarkable results for retrieval problems. In this paper, we apply attention mechanism to CNN, which aims at enhancing more relevant features that correspond to important keypoints in the input image. The generated attention-aware features are then aggregated by the previous state-of-the-art generalized mean (GeM) pooling followed by normalization to produce a compact global descriptor, which can be efficiently compared to other image descriptors by the dot product. An extensive comparison of our proposed approach with state-of-the-art methods is performed on the new challenging ROxford5k and RParis6k retrieval benchmarks. Results indicate significant improvement over previous work. In particular, our attention-aware GeM (AGeM) descriptor outperforms state-of-the-art method on ROxford5k under the “Hard” evaluation protocol.

1. Introduction

In computer vision, the task of instance-level image retrieval aims at, given a query image, retrieving all images in a large-scale database that contain the same object as the query. Traditionally, the best performing approaches relied on local invariant features such as SIFT [20] and aggregation strategies such as bag-of-words (BoW) [36], vector of locally aggregated descriptors (VLAD) [15, 2], or Fisher vector (FV) [25] built on top of these local features. The resulting representations are usually efficiently indexed and individually matched followed by a re-ranking stage.

Recently, methods based on convolutional neural networks (CNNs) have been advancing rapidly since the success of Krizhevsky *et al.* [19] in the image classification task, and research attention has shifted to features extracted by CNNs, which is also the main focus of this paper. As a first attempt, several works [4, 31, 7] proposed to use features extracted by fully connected layers and demonstrated satisfactory performance on popular retrieval benchmarks. However, state-of-the-art results were still obtained

by non-CNN-based methods and, in order to be competitive, convolutional layers were proposed as an alternative. These feature extractors possess the advantage that a compact representation of fixed length can be produced efficiently from an input image of any size and aspect ratio. Consequently, a series of papers have been written regarding various strategies to construct competitive image representations such as sum-pooled convolution (SPoC) [3] descriptors, cross-dimensional weighted (CroW) [16] descriptors, maximum activations of convolutions (MAC) [32, 39] descriptors, or regional MAC (R-MAC) [39] descriptors. These approaches, when combined with proper post-processing techniques, produced for the first time a system that competes or outperforms conventional methods based on local features.

A major drawback of the above methods is that image descriptors were directly extracted using off-the-shelf models trained for the classification task. While being efficient, it became evident that the improvement gain was limited due to their lack of learning. The first fine-tuning approach for image retrieval was proposed by Babenko *et al.* [4] using a classification loss on a new set of landmarks images better suited for the retrieval task. Later on, Gordo *et al.* [8, 9] argued that the similarity measure being optimized should coincide with the one to be used during the final task. Building on the R-MAC pipeline, the deep image retrieval (DIR) network was trained end-to-end on a clean version of the Babenko dataset using a ranking loss to achieve state-of-the-art results. Concurrently, the work of Radenović *et al.* [30] dispensed the need of manual effort to collect/clean a large-scale dataset for training by exploiting the structure-from-motion (SfM) pipeline [34] which resulted in a suitable collection of training data consisting of matching and non-matching pairs. In addition, a novel generalized mean (GeM) pooling operation was introduced offering more performance boost over their previous work [29].

Inspired by the recent work of Wang *et al.* [41] which inserts attention modules into CNNs to improve performance in the classification task, we incorporate (soft) attention mechanism by considering a two-branch network: The main branch which, same as the above works, consists

of the base architecture before the final pooling layer, and an attention branch which consists of additional layers applied to feature maps produced by various prior blocks in the base architecture in a feedforward manner. The outputs of the two branches are then combined together by the attention residual learning mechanism as in [41] to generate attention-aware features which are aggregated by the GeM operation to produce a compact image representation referred to as the attention-aware GeM (AGeM) descriptor. Due to the nature of identity mapping in residual learning, the performance of AGeM should be at least as good as its predecessor. In fact, as will be demonstrated in the experimental section below, AGeM outperforms GeM on all datasets for all evaluation protocols since the attention branch learns to successfully suppress features which correspond to irrelevant information in the input image.

The rest of this paper is organized as follows. In Section 2, we review the related work. In Section 3, we describe our proposed network architecture and introduce attention-aware generalized mean (AGeM) descriptors. The training and test datasets used for our experiments are discussed in Section 4. Finally, in Section 5, we perform an extensive evaluation comparing various state-of-the-art methods in the literature, and the paper concludes with Section 6.

2. Related work

In the past few years, CNN-based global representations have become an attractive solution for the task of image retrieval. Starting from setting the fully connected layers as feature extractors using off-the-shelf models, to switching to convolutional layers, it has now become a promising direction that good performance is achieved by fine-tuned models using convolutional layer activations as feature maps. In addition to the above mentioned works, there is a growing trend recently of utilizing various types of attention mechanism to improve accuracy. The main idea can be more or less summarized in simple terms as “some features are more important than others and should be assigned more weights”.

The idea of applying attention into deep neural networks is not new, and has already been used in many areas of deep learning, especially in tasks tackled by sequence-to-sequence networks. In computer vision, and more specifically for instance-level image retrieval, the following works are some recent examples where an attention-type network is proposed to enhance relevant features. For instance, [16] proposed CroW as a non-parametric spatial- and channel-wise weighting scheme to prevent burstiness effects, while selective convolutional descriptor aggregation (SCDA) was introduced in [42] as an unsupervised method for localizing the main object and discarding noisy background to improve performance in fine-grained image retrieval. In a very recent work, [22] proposed another aggregation method by

considering each deep feature as a heat source and utilizing the heat equation to avoid over-representation of bursty features. These approaches use a pre-trained CNN model without additional learning. On the fine-tuning side, [17] proposed to improve the R-MAC pipeline, which treats all regions equally, by employing a context-aware region-wise attention module assigning weights to regions of varying importance. The network is partially fine-tuned in the sense that the parameters of the off-the-shelf CNN model are fixed and only the parameters of the regional attention network are trained. Related to that, the attentive deep local feature (DELFF) [21] descriptor was trained using a two-step strategy by first fine-tuning a softmax-based classifier followed by fixing the features and learning a score function for the attention model. For methods which involve end-to-end fine-tuning, the attention-based pyramid aggregation network (APANet) [45] applied spatial pyramid pooling on the feature maps followed by an attention block producing scores for the regional features before aggregation, while the weighted GeM (wGeM) [44] used a single convolutional layer followed by a spatial softmax function on the feature maps before the final pooling operation to generalize GeM.

In another direction, for the closely related tasks of classification and detection, the convolutional block attention module (CBAM) [43] proposed to sequentially append a channel attention module and a spatial attention module on the feature maps for feature refinement, and showed performance improvement. Departing from these approaches, we propose a simple and straightforward network architecture that produces feature maps and attention maps of same dimensions simultaneously which are combined together for the final output. The additional attention branch is easily implementable, trainable via back-propagation, and adds only a small computational overhead.

3. Network architecture

In this section, we discuss the network architecture and pooling method, which can be applied to any CNN architecture in general.

3.1. Network and pooling

For our experiments, we choose the deep residual network [10] (specifically, ResNet-101) as our CNN architecture as it usually achieves better results than other popular networks such as AlexNet [19] or VGG [35] in image retrieval tasks.

Given an input image, we discard the final two (*i.e.* 7×7 average pooling and fully connected) layers and take the feature maps produced by the last convolutional layer as output, which is of the form $\mathcal{X} \in \mathbb{R}^{W \times H \times K}$, where K denotes the number of channels. Furthermore, we assume ReLU activation is applied so that all values of \mathcal{X} are non-negative. For $1 \leq k \leq K$, denote by $\mathcal{X}_k \in \mathbb{R}^{W \times H}$ the k -th

feature map of \mathcal{X} , we apply a pooling operation to produce a number F_k representing \mathcal{X}_k so that the input image can be represented by the vector $[F_1, \dots, F_K]^T$. This vector is then ℓ^2 -normalized which can be used to compare with other image representations by the dot product.

In the current deep learning literature, two of the simplest and most popular pooling methods are the average and max pooling operations, hence it is no surprise that they are the first to be applied in image retrieval. The corresponding vectors are commonly referred to as the SPoC [3] descriptor and MAC [32, 39, 29] descriptor, given by

$$[F_1^{(\text{SPoC})}, \dots, F_K^{(\text{SPoC})}]^T, \quad F_k^{(\text{SPoC})} = \frac{1}{|\mathcal{X}_k|} \sum_{x \in \mathcal{X}_k} x, \quad (1)$$

and

$$[F_1^{(\text{MAC})}, \dots, F_K^{(\text{MAC})}]^T, \quad F_k^{(\text{MAC})} = \max_{x \in \mathcal{X}_k} x, \quad (2)$$

respectively. Both SPoC and MAC descriptors already achieve competitively good results on standard benchmarks (see Section 5 for details). In order to further boost the performance, the generalized mean (GeM) pooling was used in [30] as a replacement for average or max pooling. The corresponding GeM descriptor is given by

$$[F_1^{(\text{GeM})}, \dots, F_K^{(\text{GeM})}]^T, \quad F_k^{(\text{GeM})} = \left(\frac{1}{|\mathcal{X}_k|} \sum_{x \in \mathcal{X}_k} x^{p_k} \right)^{\frac{1}{p_k}}, \quad (3)$$

which generalizes SPoC and MAC descriptors since (3) = (1) if $p_k = 1$ and (3) \rightarrow (2) as $p_k \rightarrow \infty$. More importantly, the GeM pooling is a differentiable operation, and hence the whole network can be trained in an end-to-end fashion.

In (3), there is a different pooling parameter p_k for each feature map \mathcal{X}_k . However, one can also use a shared parameter p for all feature maps, and it turns out this simpler option achieves slightly better results than multiple parameters as demonstrated in the experimental section of [30]. Consequently, we shall also adopt this option for our experiments.

Finally, we have $K = 2048$ for ResNet-101 so that each of the aforementioned descriptors is a 2048-D compact image representation.

3.2. Attention-aware GeM

We now describe the construction of our attention-aware GeM (AGeM) descriptor. Given an input image, the first block of the ResNet-101 architecture consists of a 7×7 convolution followed by a 3×3 max pooling to produce a feature activations output with channel size 64. Then there are four more residual blocks, denoted $\{B_2, B_3, B_4, B_5\}$, of 1×1 and 3×3 convolutional layers producing feature maps of the same size within each block. For $i \in \{2, 3, 4, 5\}$, denote by $B_{i,j}$ the j -th residual unit of B_i and $\mathcal{X}_{i,j}$ the feature

maps produced by the last layer of $B_{i,j}$. Note that $\mathcal{X}_{i,j}$ has channel size 256 (respectively, 512, 1024, and 2048) for $i = 2$ (respectively, 3, 4, and 5).

Our network architecture is made of two branches. First, there is the main branch which is exactly same as GeM before the final pooling layer that takes an input image and produces feature maps $\mathcal{X}_{5,3}$ from $B_{5,3}$ of ResNet-101. For the attention branch, we add three attention units, denoted Att1, Att2_1, and Att2_2, which are applied to feature maps $\mathcal{X}_{4,23}$, $\mathcal{X}_{5,1}$, and $\mathcal{X}_{5,2}$ produced by $B_{4,23}$, $B_{5,1}$, and $B_{5,2}$, respectively. Note that $B_{4,23}$ is the last residual unit of B_4 whereas B_5 consists of three residual units in total. The Att1 unit consists of four convolutional layers of kernel size 3×3 , 3×3 , 1×1 , and 1×1 , respectively, with stride 2 for the first layer (for downsampling) and stride 1 for the rest. The output channel size is 1024, 512, 512, and 2048, respectively, for the four layers of Att1 and, moreover, each convolutional layer is followed by BN [11] and ReLU activation, except for the last layer which is activated by the sigmoid function instead. In contrast, both Att2_1 and Att2_2 consist of only one convolutional layer with kernel size 1×1 , stride 1, and output channel size same as input channel size followed by sigmoid activation.

During the feedforward process, Att1 is applied to $\mathcal{X}_{4,23}$ producing attention maps $\mathcal{A}_{4,23}$, which is then combined with $\mathcal{X}_{5,1}$ by the Hadamard product (denoted \otimes). Likewise, Att2_1 is applied to $\mathcal{A}_{4,23} \otimes \mathcal{X}_{5,1}$ producing $\mathcal{A}_{5,1}$ and Att2_2 is applied to $\mathcal{A}_{5,1} \otimes \mathcal{X}_{5,2}$ producing $\mathcal{A}_{5,2}$ as the output of the attention branch. The final output of the network applies attention residual learning as in [41] and produces feature maps \mathcal{X} given by

$$\mathcal{X} = \mathcal{X}_{5,3} + \mathcal{A}_{5,2} \otimes \mathcal{X}_{5,3}, \quad (4)$$

followed by GeM pooling and ℓ^2 -normalization forming a compact 2048-D vector as the AGeM descriptor of the input image. The overall architecture is illustrated in Figure 1.

3.3. Loss function and whitening

In fine-tuning the network for image retrieval, three popular loss functions have been commonly used.

In one of the very first fine-tuning approaches proposed by Babenko *et al.* [4], models pre-trained on the ImageNet dataset [33] were re-trained on an external set of labelled landmark images using a classification loss. This simple strategy already resulted in a big improvement over off-the-shelf networks.

Later on, Gordo *et al.* [8, 9] showed that the results could be further improved by learning image representations that are well-suited for the retrieval task. To this end, the triplet loss was used during training instead, defined by

$$L(q, p, n) = \frac{1}{2} \max\{0, \tau + \|F(q) - F(p)\|^2 - \|F(q) - F(n)\|^2\}, \quad (5)$$

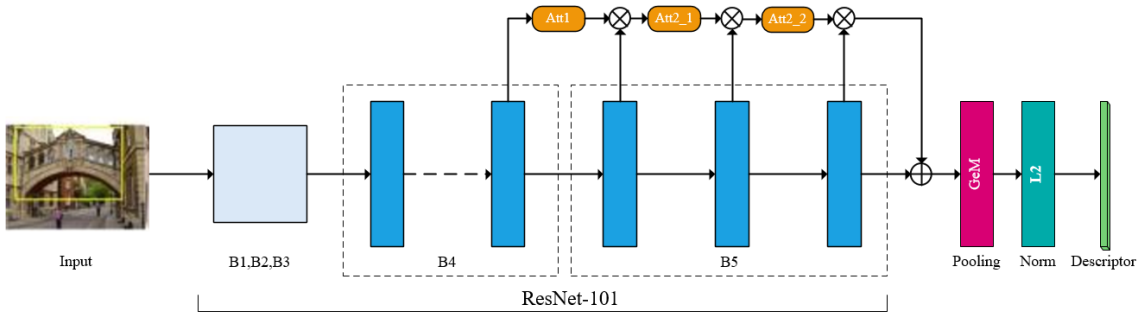


Figure 1. A general overview of our proposed network architecture.

where for a given query image q , p denotes a positive image, n denotes a negative image, and τ is a margin hyperparameter controlling the desired difference between the distances of the representations.

Finally, there is the contrastive loss used by Radenović *et al.* in [29, 30]. In this case, each training input consists of a pair of images (i, j) and a label $Y(i, j) \in \{0, 1\}$, where $Y(i, j) = 1$ if i and j are matching and 0 otherwise. The loss function is then defined by

$$L(i, j) = \begin{cases} \frac{1}{2} \|F(i) - F(j)\|^2, & Y(i, j) = 1 \\ \frac{1}{2} (\max\{0, \tau - \|F(i) - F(j)\|\})^2, & Y(i, j) = 0 \end{cases} \quad (6)$$

where again τ is a margin hyperparameter controlling the distance of non-matching pairs. As suggested in [30], contrastive loss converges at higher performance when accompanied by the GeM pooling.

Another important component one often adds to the design of a retrieval system is the PCA and whitening of image descriptors, which has been shown to be very powerful since the work of Jégou *et al.* [13]. There are two typical ways PCA and whitening can be implemented as part of a retrieval pipeline. On one hand, Gordo *et al.* [8, 9] proposed to append a fully connected layer (with bias) at the end of the network after the pooling layer to act as the mean shifting and projection so that PCA is learned together with the CNN in an end-to-end manner. In contrast, based on experimental results, Radenović *et al.* [29, 30] preferred to rather learn the discriminative whitening as a post-processing step after the fine-tuning of the CNN is finished.

Since our work is closely related to that of GeM, we shall use the contrastive loss to first optimize the CNN weights, and then perform the whitening transform using the available training pairs.

4. Datasets

In this section, we briefly describe the training and test datasets to be used for fine-tuning and evaluating our model.

4.1. Training set

For fair comparison, we will be using the same training set as Radenović *et al.* in [29, 30], derived from a large-scale set of 7.4 million images downloaded from Flickr. The original dataset was used in the work of Schönberger *et al.* [34] for 3D reconstruction from a single image. As an outcome of image retrieval and structure-from-motion reconstruction system, images are clustered and a 3D model is constructed for each cluster. The final set, after removing overlapping images and images that belong to the test set, consists of 551 clusters/models for training and 162 clusters/models for validation for a total of around 120k images.

To make use of the contrastive loss (6), an automatic selection process was proposed in [29, 30] to create tuples where each tuple consists of a query image, one hard positive image matching the query, and a pool of hard negative images with at most one image per cluster. During the training process, positive examples remain fixed while negative examples are re-mined every epoch.

4.2. Test set

We test our method on the revised version of the popular Oxford5k [26] and Paris6k [27] retrieval benchmark datasets, referred to as ROxford5k and RParis6k [28], respectively.

The original Oxford5k and Paris6k datasets consist of 5,063 and 6,392 images of size 1024×768 . Each dataset contains 55 queries depicting 11 landmarks evenly (*i.e.* 5 queries per landmark), where each landmark comes with a ground truth list of images labelled as good, ok, junk, or absent. Given a query image, the goal is to retrieve all good and ok images (treated as positives) from the ground truth list while junk images are ignored and absent images are

treated as negatives. The performance is measured by mean average precision (mAP) over all 55 queries.

Despite the popularity, there are known drawbacks related to the annotation error, size, and challenge level of the datasets. Consequently, it has become difficult to draw conclusions for methods which achieve almost perfect results. To address these issues, ROxford5k and RParis6k were introduced in [28] as a replacement for future comparisons. The major changes are: (1) New annotation for both datasets were created; (2) For each dataset, 15 additional challenging queries were added for a total of 70 queries; (3) Images in the ground truth list were relabelled as easy, hard, unclear, or negative. Three evaluation protocols (Easy, Medium, Hard) were defined, where the Easy setup only requires easy images to be retrieved, the Medium setup counts both easy and hard images as positives, and the Hard setup strictly asks for hard images only.

In the subsequent experiments, we only evaluate according to the Medium and Hard protocols because the Easy setup is close to the original protocol and hence less challenging where high scores can be achieved by the current state-of-the-art models. In addition, we crop the query images with the provided bounding boxes before feeding to the network as per the standard evaluation protocols.

5. Experiments

In this section, we discuss implementation details and evaluate the performance of various methods.

5.1. Preliminary results

Implementation details. For better comparison, all results are produced using the same hyperparameter setting which most closely resembles that of [30]. We use PyTorch [23] for fine-tuning the network. The weights of ResNet-101 are initialized by model pre-trained on the ImageNet dataset [33] and the pooling parameter is initialized at $p = 2.92$, while the attention layers have weights started by Xavier initialization [6]. We use Adam [18] as optimizer with initial learning rate $\ell_0 = 10^{-6}$, exponential decay $\ell_0 \exp(-0.01k)$ over epoch k , momentum 0.9, weight decay 10^{-4} , and contrastive loss with margin 0.85. For the pooling parameter p and the parameters of the attention layers, the initial learning rates are set to be 10^{-5} and 10^{-3} , respectively, and there is no weight decay for p . Training is done for at most 60 epochs each containing 2,000 tuples with batch size 10. Every tuple consists of 1 query image, 1 positive image, and 5 negative images selected from a pool of 20,000 negative images. All images are resized before feeding to the network so that the longer side has size 512 while keeping the original aspect ratio. The whole process takes about 30 hours (about 30 minutes for 1 epoch) on a single NVIDIA Tesla P100 GPU with 16 GB of memory,

and the best model is selected based on performance on the validation set.

Multi-scale representation. During test time, we resize the input images to 1,024 pixels in the longer side without distorting the original aspect ratio. Furthermore, we adopt the multi-scale scheme, first proposed in the work of Gordo *et al.* [8, 9] and later also used in [30], to enhance retrieval performance by extracting descriptors at different scales with scaling factors 1, $\frac{1}{\sqrt{2}}$, and $\frac{1}{2}$. These descriptors are then combined into a single vector by average pooling followed by ℓ^2 -normalization. For GeM and our AGeM descriptors, generalized mean pooling is used instead, where the pooling parameter is set to be the value learned during fine-tuning of the network. The whitening transform is then learned on the final multi-scale descriptors.

In Figure 2, we present the evaluation results using our AGeM descriptors together with GeM, MAC, and SPoC descriptors on the ROxford5k and RParis6k datasets as training progresses. All descriptors are accompanied by multi-scale representation and discriminative whitening learned on the training pairs.

From the plots in Figure 2, we observe that AGeM and GeM outperform both MAC and SPoC from beginning until the end. As for the comparison between AGeM and GeM, despite the wilder fluctuations of the purple curves (corresponding to AGeM) due to the larger initial learning rate on the weights of attention layers, the dominance is clear over the red curves (corresponding to GeM), especially on the RParis6k dataset. In general, it appears that the best performance on ROxford5k and on the validation set occurs around the 40-th epoch, whereas for RParis6k the performance usually degrades in the second half of the training. If one aims at achieving good accuracy on RParis6k only, we suggest reducing the training time in half and take the best model from the first 30 epochs.

5.2. Comparison with state-of-the-art

We now apply a number of standard post-processing techniques to boost the performance, and extensively compare our results with some state-of-the-art methods.

Query expansion. It has now become a common practice to improve the retrieval results by combining query expansion (QE) with CNN descriptors since the work of [5]. The simplest form of QE works as follows: Given a query image, an initial search is performed and the N top-ranked images are retrieved. The descriptors of these N images are then combined with the descriptor of the original image by average aggregation and ℓ^2 -normalization, and the resulting vector is used for a second search. We refer to this simple way of combining descriptors as average query expansion (AQE).

Database augmentation. Like QE, one can also apply the same technique on the database side by replacing every im-

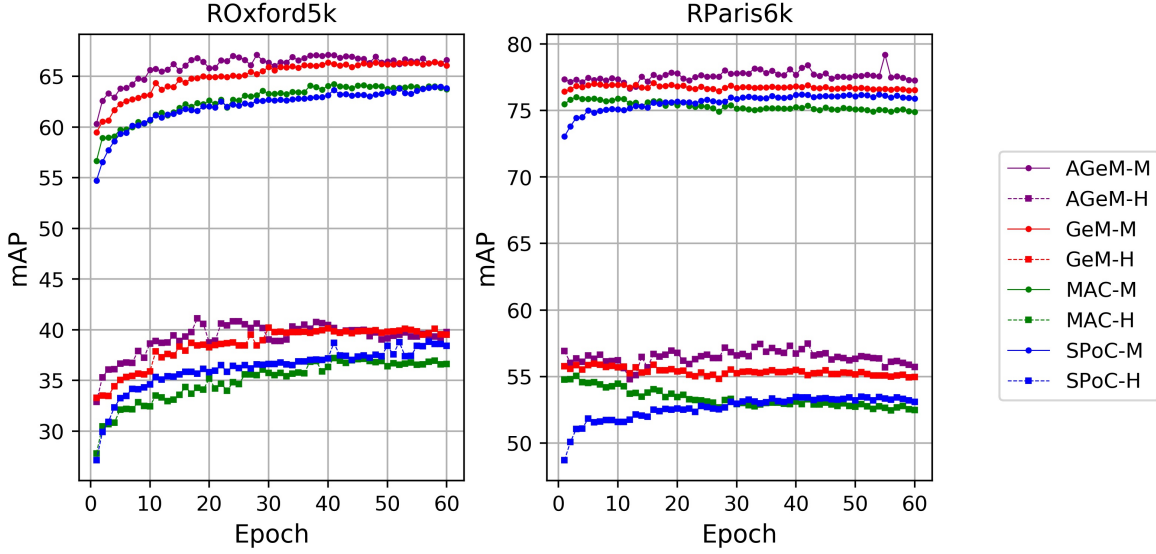


Figure 2. Performance comparison of AGeM, GeM, MAC, and SPoC descriptors on the ROxford5k and RParis6k datasets during training using Medium (-M) and Hard (-H) evaluation protocols.

age descriptor by a combination of itself and the descriptors of its closest neighbors. This strategy is known as database augmentation (DBA), introduced in the works of [40, 1] and shown to be very effective in [8, 9].

In Figure 3, we evaluate the effects of AQE and DBA with respect to the number of neighbors used on the ROxford5k and RParis6k datasets using the Medium and Hard setups. We observe that 2 seems to be the best number of neighbors for DBA regardless of the dataset or evaluation protocol. For ROxford5k where many queries have very few positive matches in the dataset, choosing a large number of neighbors for AQE can significantly degrade the performance, whereas for RParis6k a larger number of neighbors seems to offer improvement since all queries have many relevant images to be retrieved. Consequently, we suggest choosing a small number of neighbors (*i.e.* 1 or 2) for the Oxford dataset and a large number of neighbors (*i.e.* 40 or 50) for the Paris dataset.

Weighted QE and DBA. In AQE, all retrieved images have equal weight when contributing to the combined descriptor. This is suboptimal as, intuitively, images with higher rank should be assigned a larger weight. To address this issue, α QE was introduced in [30] where for a query image q , the weight assigned to a top-ranked image i is given by $(F(q)^T F(i))^\alpha$. Likewise, one can also adopt a similar weighting scheme for DBA.

In Figure 4, we evaluate the effects of the exponents α and β used in the weights of QE and DBA, respectively. Based on the curves in Figure 4, we settle for $\beta = 1$ and, perhaps surprisingly, $\alpha = 0$, *i.e.* when weighted DBA is

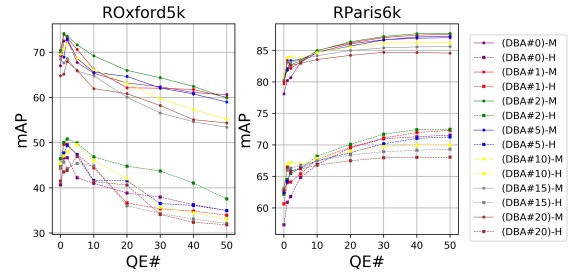


Figure 3. Performance as a function of the # of neighbors used for AQE (QE#) for different values of the # of neighbors used for DBA (DBA#) using Medium (-M) and Hard (-H) setups.

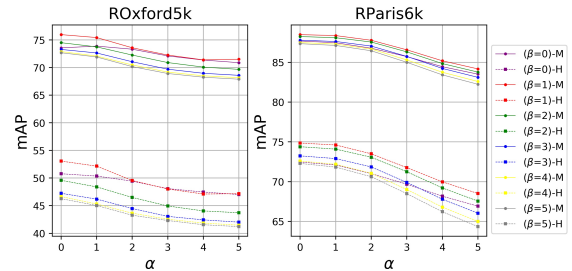


Figure 4. Performance as a function of α used for QE weights for different values of β used for DBA weights.

used, the best complement on the query side happens to be AQE.

Diffusion. Introduced in the work of [12], diffusion (DFS)

is a recent performance-boosting method aiming at recovering small objects. When applied on top of compact CNN descriptors, a significant improvement is achieved since it is quite common, especially under the new evaluation protocols, that the object of interest only covers a small part of the image.

In Table 1, we compare our proposed method against the state-of-the-art. We do not include results obtained by off-the-shelf models since they almost always perform worse. In the top section of Table 1 corresponding to results without post-processing techniques, the first two rows represent local-feature methods based on Hessian-affine (HesAff) features [24], RootSIFT (rSIFT) [1] descriptors, or deep local features (DELFF) [21] encoded by aggregated selective match kernel (ASMK*) [37] with spatial verification (SP) [26], whereas the rest represents various global-CNN-feature methods. In this case, the best performance on ROxford5k is achieved by local features while global CNN features seem to dominate on RParis6k, a conclusion consistent with the message of [28] that both worlds (local and global CNN) have their own benefits. Our proposed AGeM method, although not being the best at this stage, does offer non-trivial improvement over GeM especially on RParis6k.

On the other hand, the middle section of Table 1 corresponds to results with post-processing techniques applied on top of the features, where global-CNN-feature methods are equipped with DBA, QE, and/or DFS as described earlier and local-feature methods use Hamming query expansion (HQE) [38] as a combination of QE with the Hamming embedding (HE) technique [14]. In this case, we notice that AGeM outperforms all other methods by a huge margin when combined with DFS. One unusual observation we make is that there seems to be a big discrepancy between our own implementation of GeM with DFS (marked with \star) compared to results reported by the authors in Table 5 of [28] on ROxford5k. It is not clear to us at the moment what the cause is since, according to the authors' results (marked with \dagger), DFS only adds very little improvement to GeM on ROxford5k. Another interesting observation we make is that, according to our experiments, MAC seems to perform better than GeM on RParis6k when combined with DFS.

Finally, the bottom section of Table 1 reports the previous state-of-the-art performance achieved by first obtaining a verified list of relevant images using local features, and then starting the global-CNN-feature method from the geometrically verified images. Even in this case, our single-method approach outperforms two of the three combinations and is on par with the last one. In particular, we establish the new state-of-the-art on ROxford5k under the Hard evaluation protocol with an mAP of 58.4.

6. Conclusion

In this work, we have presented an effective method to incorporate attention mechanism with CNNs for image retrieval. The proposed approach generates attention-aware features which can be combined with the previous state-of-the-art GeM pooling method to produce a compact global descriptor with minimal overhead. The whole network can be trained end-to-end efficiently providing a substantial boost in retrieval accuracy on the challenging ROxford5k and RParis6k benchmark datasets. The result achieved by our approach outperforms or is competitive even with complex time-consuming state-of-the-art methods based on local features and spatial verification. We intend to further exploit different weighting schemes in the future.

References

- [1] R. Arandjelović and A. Zisserman. Three things everyone should know to improve object retrieval. *CVPR*, 2012.
- [2] R. Arandjelović and A. Zisserman. All about vlad. *CVPR*, 2013.
- [3] A. Babenko and V. Lempitsky. Aggregating deep convolutional features for image retrieval. *ICCV*, 2015.
- [4] A. Babenko, A. Slesarev, A. Chigorin, and V. Lempitsky. Neural codes for image retrieval. *ECCV*, 2014.
- [5] O. Chum, J. Philbin, J. Sivic, M. Isard, and A. Zisserman. Total recall: Automatic query expansion with a generative feature model for object retrieval. *ICCV*, 2007.
- [6] X. Glorot and Y. Bengio. Understanding the difficulty of training deep feedforward neural networks. *AISTATS*, 2010.
- [7] Y. Gong, L. Wang, R. Guo, and S. Lazebnik. Multi-scale orderless pooling of deep convolutional activation features. *ECCV*, 2014.
- [8] A. Gordo, J. Almazan, J. Revaud, and D. Larlus. Deep image retrieval: Learning global representations for image search. *ECCV*, 2016.
- [9] A. Gordo, J. Almazan, J. Revaud, and D. Larlus. End-to-end learning of deep visual representations for image retrieval. *IJCV*, 2017.
- [10] K. He, X. Zhang, S. Ren, and J. Sun. Deep residual learning for image recognition. *CVPR*, 2016.
- [11] S. Ioffe and C. Szegedy. Batch normalization: Accelerating deep network training by reducing internal covariance shift. *ICML*, 2015.
- [12] A. Iscen, G. Tolia, Y. Avrithis, T. Furon, and O. Chum. Efficient diffusion on region manifolds: Recovering small objects with compact cnn representations. *CVPR*, 2017.
- [13] H. Jégou and O. Chum. Negative evidences and co-occurrences in image retrieval: The benefit of pca and whitening. *ECCV*, 2012.
- [14] H. Jégou, M. Douze, and C. Schmid. Hamming embedding and weak geometric consistency for large scale image search. *ECCV*, 2008.
- [15] H. Jégou, M. Douze, C. Schmid, and P. Pérez. Aggregating local descriptors into a compact image representation. *CVPR*, 2010.

Method	ROxf-M	ROxf-H	RPar-M	RPar-H
\dagger HesAff-rSIFT-ASMK* + SP	60.6	36.7	61.4	35.0
\dagger DELF-ASMK* + SP	67.8	43.1	76.9	55.4
\dagger DIR	60.9	32.4	78.9	59.4
\dagger GeM (MatConvNet)	64.7	38.5	77.2	56.3
\dagger GeM (PyTorch)	65.3	40.0	76.6	55.2
*SPoC	63.8	38.8	76.1	53.4
*MAC	64.0	37.0	75.4	53.3
*GeM	66.4	40.1	76.8	55.5
AGeM	67.0	40.7	78.1	57.3
\dagger HesAff-rSIFT-HQE + SP	71.3	49.7	70.2	45.1
\dagger DELF-HQE + SP	73.4	50.3	84.0	69.3
\dagger DIR + α QE	64.8	36.8	82.7	65.7
\dagger DIR + DFS	69.0	44.7	89.5	80.0
\dagger GeM + α QE	67.2	40.8	80.7	61.8
\dagger GeM + DFS	69.8	40.5	88.9	78.5
*SPoC + α QE	69.5	44.2	84.0	65.7
*SPoC + DFS	63.8	38.8	86.4	73.1
*MAC + α QE	70.5	42.9	85.3	68.3
*MAC + DFS	76.2	51.1	88.6	79.5
*GeM + α QE	71.6	45.7	85.7	69.2
*GeM + DFS	78.4	54.0	88.5	78.8
AGeM + DBA + QE	73.6	50.8	87.7	72.5
AGeM + β DBA + α QE	76.0	53.1	88.5	74.9
AGeM + DFS	79.7	55.8	89.6	80.5
AGeM + β DBA + α QE + DFS	79.4	58.4	91.3	82.1
\dagger HesAff-rSIFT-ASMK* + SP \rightarrow DIR + DFS	80.2	54.8	92.5	84.0
\dagger HesAff-rSIFT-ASMK* + SP \rightarrow GeM + DFS	79.1	52.7	91.0	81.0
\dagger DELF-ASMK* + SP \rightarrow DIR + DFS	75.0	48.3	90.5	81.2

Table 1. Performance evaluation (mAP) on ROxford5k (ROxf) and RParis6k (RPar) using Medium (-M) and Hard (-H) evaluation protocols without and with post-processing techniques. For methods other than AGeM, the \dagger symbol denotes results from the original papers or trained models released by the authors whereas \star represents our reproduction using publicly available source codes.

- [16] Y. Kalantidis, C. Mellina, and S. Osindero. Cross-dimensional weighting for aggregated deep convolutional features. *ECCV*, 2016.
- [17] J. Kim and S.-E. Yoon. Regional attention based deep feature for image retrieval. *BMVC*, 2018.
- [18] D. Kingma and J. Ba. Adam: A method for stochastic optimization. *ICLR*, 2015.
- [19] A. Krizhevsky, I. Sutskever, and G. Hinton. Imagenet classification with deep convolutional neural networks. *NIPS*, 2012.
- [20] D. Lowe. Distinctive image features from scale-invariant keypoints. *IJCV*, 2004.
- [21] H. Noh, A. Araujo, J. Sim, T. Weyand, and B. Han. Large-scale image retrieval with attentive deep local features. *ICCV*, 2017.
- [22] S. Pang, J. Ma, J. Xue, J. Zhu, and V. Ordonez. Deep feature aggregation and image re-ranking with heat diffusion for image retrieval. *Trans. Multimed.*, 2018.
- [23] A. Paszke, S. Gross, S. Chintala, G. Chanan, E. Yang, Z. DeVito, Z. Lin, A. Desmaison, L. Antiga, and A. Lerer. Automatic differentiation in pytorch. *NIPS*, 2017.
- [24] M. Perdoch, O. Chum, and J. Matas. Efficient representation of local geometry for large scale object retrieval. *CVPR*, 2009.
- [25] F. Perronnin, Y. Liu, J. Sánchez, and H. Poirier. Large-scale image retrieval with compressed fisher vectors. *CVPR*, 2010.
- [26] J. Philbin, O. Chum, M. Isard, J. Sivic, and A. Zisserman. Object retrieval with large vocabularies and fast spatial matching. *CVPR*, 2007.
- [27] J. Philbin, O. Chum, M. Isard, J. Sivic, and A. Zisserman. Lost in quantization: Improving particular object retrieval in large scale image databases. *CVPR*, 2008.
- [28] F. Radenović, A. Iscen, G. Tolias, Y. Avrithis, and O. Chum. Revisiting oxford and paris: Large-scale image retrieval benchmarking. *CVPR*, 2018.
- [29] F. Radenović, G. Tolias, and O. Chum. Cnn image retrieval learns from bow: Unsupervised fine-tuning with hard examples. *ECCV*, 2016.

- [30] F. Radenović, G. Tolias, and O. Chum. Fine-tuning cnn image retrieval with no human annotation. *TPAMI*, 2018.
- [31] A. Razavian, H. Azizpour, J. Sullivan, and S. Carlsson. Cnn features off-the-shelf: An astounding baseline for recognition. *CVPR*, 2014.
- [32] A. Razavian, J. Sullivan, S. Carlsson, and A. Maki. Visual instance retrieval with deep convolutional networks. *ITE Trans. MTA*, 2016.
- [33] O. Russakovsky, J. Deng, H. Su, J. Krause, S. Satheesh, S. Ma, Z. Huang, A. Karpathy, A. Khosla, M. Bernstein, A. Berg, and F. Li. Imagenet large scale visual recognition challenge. *IJCV*, 2015.
- [34] J. Schönberger, F. Radenović, O. Chum, and J.-M. Frahm. From single image query to detailed 3d reconstruction. *CVPR*, 2015.
- [35] K. Simonyan and A. Zisserman. Very deep convolutional networks for large-scale image recognition. *ICLR*, 2015.
- [36] J. Sivic and A. Zisserman. Video google: A text retrieval approach to object matching in videos. *ICCV*, 2003.
- [37] G. Tolias, Y. Avrithis, and H. Jégou. Image search with selective match kernels: Aggregation across single and multiple images. *IJCV*, 2015.
- [38] G. Tolias and H. Jégou. Visual query expansion with or without geometry: Refining local descriptors by feature aggregation. *Pattern Recognit.*, 2014.
- [39] G. Tolias, R. Sivic, and H. Jégou. Particular object retrieval with integral max-pooling of cnn activations. *ICLR*, 2016.
- [40] P. Turcot and D. Lowe. Better matching with fewer features: The selection of useful features in large database recognition problems. *ICCV*, 2009.
- [41] F. Wang, M. Jiang, C. Qian, S. Yang, C. Li, H. Zhang, X. Wang, and X. Tang. Residual attention network for image classification. *CVPR*, 2017.
- [42] X.-S. Wei, J.-H. Luo, J. Wu, and Z.-H. Zhou. Selective convolutional descriptor aggregation for fine-grained image retrieval. *TIP*, 2017.
- [43] S. Woo, J. Park, J.-Y. Lee, and I. Kweon. Cbam: Convolutional block attention module. *ECCV*, 2018.
- [44] X. Wu, G. Irie, K. Hiramatsu, and K. Kashino. Weighted generalized mean pooling for deep image retrieval. *ICIP*, 2018.
- [45] Y. Zhu, J. Wang, L. Xie, and L. Zheng. Attention-based pyramid aggregation network for visual place recognition. *ACM-MM*, 2018.